Available online at www.sciencedirect.com
SCIENCE DIRECT®
Nuclear Physics A 742 (2004) 363–379
NUCLEAR PHYSICS A
www.elsevier.com/locate/npe

Fully consistent semi-classical treatment of vortex–nucleus interaction in rotating neutron stars

Paola Donati *, Pierre M. Pizzochero

Dipartimento di Fisica, Università degli Studi di Milano, and Istituto Nazionale di Fisica Nucleare, Sezione di Milano, via Celoria 16, 20133 Milano, Italy

Received 1 April 2004; received in revised form 1 June 2004; accepted 6 July 2004

Available online 28 July 2004

Abstract

We present the first realistic and fully consistent model to study the vortex–nucleus interaction in the inner crust of a rotating neutron star, where a gas of unbound superfluid neutrons threaded by vortex lines coexists with a lattice of neutron-rich nuclei. Within the framework of the local density approximation, the model determines unambiguously the structure and radius of the vortex core along the crust, and takes into account all energy contributions to evaluate the vortex–nucleus configuration with lowest energy. The results show that, quite independent from the pairing interaction used, pinning of vortices on nuclei occurs only in the deepest layers of the crust and even there the average pinning forces are quite weak. If confirmed by complete quantum calculations, such a limited region of weak nuclear pinning may be relevant to the explanation of pulsar glitches.

PACS: 26.60.+c; 97.60.Gb

Keywords: Neutron stars; Pinning; Glitches; Vortex

* Corresponding author.
E-mail address: paola.donati@mi.infn.it (P. Donati).

0375-9474/$ – see front matter
doi:10.1016/j.nuclphysa.2004.07.002

1. Introduction

One of the most challenging problems of modern nuclear physics is to explore and understand the behavior of matter under extreme conditions of temperature and density, and therefore determine the corresponding equation of state. Its knowledge is of key importance for the physics of the early universe as well as for remarkable astrophysical phenomena such as the gravitational collapse of massive stars and subsequent supernova explosion, the formation and properties of compact stars, etc.

On the Earth, the properties of dense matter in the high-temperature domain are probed by heavy-ion colliders. Nature, on the other hand, has provided us with a large number of compact stellar objects which contain matter in one of the densest forms found in the Universe, namely neutron stars. The enormous gravitational pull compresses matter to central densities that are up to one order of magnitude higher than what found in stable atomic nuclei (the nuclear saturation density $\rho_0 = 2.8 \times 10^{14}$ g/cm^3), rendering neutron stars unique astrophysical probes of cold (the thermal energies in neutron stars are much lower than the typical excitation energies) and stable super-dense matter.

Recent observations have shown that neutron stars are not rare stellar objects, but that their number in our Galaxy is probably as large as 10^9. A rotating neutron star is born with an enormous store of angular momentum and rotational energy (estimated to be $\sim 10^{55}$ MeV for the Crab Pulsar), which it radiates away slowly over millions of years by electromagnetic radiation and a wind of electron–positron pairs. The main characteristic of a pulsar is the emission of short pulses of radiation at very regular intervals, with periods ranging from 1.6 ms to a few seconds. Although the star gradually spins down due to the radiative processes, some very interesting irregularities have been observed in the rotational frequencies of several pulsars, which can only be related to sudden changes inside the neutron star itself. Numerous models have been proposed to explain the origin of these sudden frequency spin-ups, called glitches, since they were first observed in 1969. These include starquakes, vortex pinning, magnetospheric instabilities and instabilities in the motion of superfluid neutrons.

A promising model [1] developed to explain the observed glitch behavior of pulsars is based on the formation of vortex lines in the neutron superfluid that is expected to exist inside the star, following the dripping of neutrons out of nuclei. Indeed, in the inner crust, which extends from the neutron drip density ($\rho_d \simeq 4 \times 10^{11}$ g/cm^3) to the density where individual nuclei disappear ($\rho_c \simeq 0.6\rho_0$), a gas of unbound neutrons coexists with a Coulomb lattice of heavy and very neutron-rich nuclei. As in the BCS theory of superconductivity, the neutrons with energies close to the Fermi energy are believed to pair and form an isotropic ^{1}S$_0$ superfluid. In a rotating neutron star, however, the neutron superfluid cannot co-rotate rigidly with the normal (i.e., non-superfluid) components of the star, because superfluid flow must be irrotational.

The only way a superfluid can reproduce macroscopically a rigid rotation is by developing an array of microscopic linear vortices, singular regions around which the superfluid circulation is non-zero. With a uniform density of vortices per unit area $n_{\rm vort} = 2m_n\Omega/(\pi\hbar)$ (this is the Feynman–Onsager relation [2], where m_n is the neutron mass and Ω is the star rotational frequency), the macroscopic velocity field, $\langle\vec{v}\rangle$, satisfies the rigid rotation relation $\vec{\nabla} \times \langle\vec{v}\rangle = 2\vec{\Omega}$. The macroscopic velocity is an average over regions

containing several vortices; for example, for the Crab Pulsar the mean distance between vortices is of the order of $n_{\rm vort}^{-1/2} \sim 10^{-2}$ cm, which sets the minimum scale for the macroscopic approach. Quantization of circulation around the vortices implies that the angular momentum is quantized as well, each vortex representing a quantum of angular momentum. This means that a change in the vortex-line distribution, either by a distortion of the configuration of the existing lines or by the creation of new lines or by the destruction of existing ones, corresponds to a variation in the macroscopic velocity field.

As pointed out in Ref. [1], if the vortices in the inner crust pin to the nuclei of the lattice, they are unable to migrate outwards; therefore the angular velocity of the superfluid, Ω_s, cannot change since the vortex distribution is fixed. As the angular velocity of the normal component of the star (which includes the nuclear lattice) decreases due to electromagnetic braking, the difference between the angular velocities of the superfluid and the crust grows. This differential motion will be the source of drag forces (Magnus force) which eventually, when they overcome the pinning force, could cause glitches: indeed, according to the model, the simultaneous unpinning of many vortex lines represents a sudden transfer of the angular momentum stored in the vortices from the superfluid to the (normal) outer crust and surface, and this in turn yields the observed speed-up of the rotational frequency. The appeal of this model, if successful, is that pulsar glitches would be a direct evidence of neutron superfluidity inside neutron stars and thus, indirectly, they could represent a macroscopic probe of the microscopic nucleon–nucleon residual interaction.

A quantitative investigation of the effects proposed in the model is complicated since, among other issues, the interaction of a single nucleus with a vortex line should be determined by computing the changes of the system total energy as a function of the relative position between vortex and nucleus. A simpler approach is to calculate only the pinning energy [3–5], defined as the difference in energy between two extreme configurations: one with the vortex line fixed on a nucleus (nuclear pinning) and the other with the vortex line in a position equidistant between two nuclei (interstitial pinning). The results of these calculations are important to determine which kind of pinning is energetically favored along the inner crust, as well as to evaluate the (average) pinning force.

Previous studies all predict nuclear pinning in the deeper layers of the inner crust, but they give quite different values for the pinning energies in these regions. The first estimate [3] considered only the difference in pairing condensation energy in the two cited configurations, using a quite simplified model with uniform densities for both the nucleus and the neutron gas. Later, it was pointed out [4] that also the difference in kinetic energy has to be taken into account, and that it is necessary to use a realistic density profile for the nuclei present in the inner crust [6], in order to consider their effect on the pairing energies. However, the method used in Ref. [4] to evaluate the pairing properties of the neutron superfluid is based on the Landau–Ginzburg approximation, which is far from being applicable in the inner crust. Indeed, the temperature there is practically zero ($T \sim 0.01$ MeV), while in the Landau–Ginzburg approach the temperature should be close to the critical value, that is $T_c \sim 0.5$ MeV. As a consequence, the authors of Ref. [4] must artificially rescale their results by large factors in order to reproduce experimental condensation energies for ordinary nuclei.

To overcome this difficulty, a different approach was presented later [5], in which the Thomas–Fermi model based on the Local Density Approximation (LDA) was used to de-

scribe the pairing properties of the system. The rationale behind this choice is that, although unable to describe correctly the density tail of a system, where the density goes to zero, the LDA is expected to yield reasonable results for quantities averaged over the whole system such as the energies, which are integrated over the Wigner–Seitz unit cells. In Ref. [5] nuclear pinning was also found to occur at large densities, as in previous studies, but the calculated pinning energies were one order of magnitude lower than the ones obtained before. In spite of its known limitations, the LDA approach is to date the most satisfying one, especially if one keeps in mind the difficulties of performing a quantum calculation for the complicated geometries of the vortex–nucleus configurations. When applied to thermal properties of the inner crust of neutron stars (such as the specific heat of the nuclear-lattice plus neutron-gas system), the LDA method yields results that are qualitatively similar to and compatible with those coming from a complete quantum calculation. At the quantitative level, of course, the results are different as a consequence of proximity effects connected with the non-local nature of pairing. In the case of the specific heat, the quantum results somehow 'smooth out' those coming from the LDA [7].

The results of Ref. [5], however, are not complete nor consistent, due to some assumptions that are basically incorrect. The first one is the definition of the vortex core which, as in all previous calculations, is assumed to be the superfluid coherence length ξ. This quantity represents the distance from the vortex axis where the increase of kinetic energy, due to the vorticose rotation of superfluid neutrons, equals the decrease in condensation energy, due to the pairing of neutrons in Cooper pairs. The rationale behind this choice is that outside the radius ξ the negative condensational energy dominates the kinetic one, so that it is energetically more convenient for matter to be superfluid and move irrotationally around the vortex axis; conversely, inside this radius matter is in the normal state and at rest in a frame comoving with the star normal component. However, this choice of the vortex core is inconsistent with the Thomas–Fermi model, which describes the hydrostatic equilibrium of a fermion gas subject to position-dependent potentials. Indeed, it is easy to show that the pressures of the normal and superfluid phases, when calculated with the Thomas–Fermi approach, are different at $r = \xi$ so that the two phases cannot coexist there because they are not in mechanical equilibrium. A second criticism to Ref. [5] is related to the structure of the vortex line itself, since the core has always been taken as made of normal matter. This is not necessarily true, because there exists the alternative possibility of a core empty of matter, while still preserving hydrostatic equilibrium. Which one of the two scenarios, normal or empty core, is actually adopted by the system depends on which corresponds to the minimum total energy. One final criticism to the results of Ref. [5] is that only the condensational and kinetic energy were included, while neglecting the internal contribution to the total energy.

The previous issues were answered by us in a recent Letter [8], where we presented a fully consistent semi-analytical schematic model to study the vortex–nucleus interaction. In the framework of the local density approximation and assuming a constant pairing gap and a square-well nuclear potential, the model takes consistently into account all energy contributions: condensational, kinetic and internal. It also determines unambiguously, by global energy considerations and preserving hydrostatic equilibrium, the structure and radius of the vortex core. The results showed that, depending on the density and on the vortex–nucleus configuration, the vortex cores could be either small and empty of matter

or large and made of normal matter. More important, irrespective of the value of the pairing gap, only interstitial pinning took place all along the inner crust, which is surprising and totally in contrast with all previous calculations. However, although the calculations performed in Ref. [8] are perfectly correct, the conclusions reached there are *not* due to a subtle point. Indeed, when comparing the energies of the different configurations we neglected a term related to the small but crucial change in particle number, which follows from keeping the chemical potential fixed.

In the present paper, we both correct the conclusions of Ref. [8] and develop a more realistic version of the model, which goes beyond the schematic assumption of constant pairing gap and square-well nuclear potential. Namely, we introduce density-dependent gaps obtained from different nucleon–nucleon pairing interactions (Argonne and Gogny) as well as Woods–Saxon potentials to represent the peculiar density structure of the nuclei inside the inner crust [6]. The results show that the vortex cores are always made of normal matter and have quite large radii. As in previous calculations, nuclear pinning is favored deep inside the inner crust, but at quite larger densities than what found so far and with average pinning forces that are quite small. If confirmed by complete quantum calculations, the presence of only a *limited region of weak nuclear pinning* may be relevant to the explanation of pulsar glitches, and its consequences on the models for glitches should definitely be tested.

In Section 2 we present in detail our physical model, while in Section 3 we give the numerical results of the calculations using Argonne and Gogny pairing gaps. We finally end the paper with some general conclusions.

2. Physical model

The microscopic structure of the inner crust of neutron stars was studied in Ref. [6] for different average baryon densities ρ_B in the framework of the Wigner–Seitz (WS) approximation. That is, the regular lattice of neutron-rich nuclei is assumed to be divided into unit spherical cells of radius R_{WS}, each containing a total number N of neutrons and with a single neutron-rich nucleus of radius R_N and diffusivity a at its center, characterized by Z protons and N_{bound} bound neutrons. The gas of unbound neutrons is characterized by a number density n_G far away from the nucleus, and their total number in each cell is $N_{\mathrm{free}} = N - N_{\mathrm{bound}}$. In our model, however, we will consider vortex configurations involving two WS-cells so that, in order to calculate consistently the energy differences, we must take *cubic* cells with side $L_{\mathrm{WS}} = 2R_{\mathrm{WS}}$. As a consequence, the number of unbound neutrons must be renormalized to $N'_{\mathrm{free}} = 6N_{\mathrm{free}}/\pi$. In Table 1 we report the parameters associated to five zones along the inner crust taken from Ref. [6]. More exotic nuclear shapes, called 'pasta' and 'lasagna' phases, could appear in the inner crust for densities above $\rho_c \sim 10^{14}$ g/cm^3, that is deeper than the zones we are going to consider in this paper.

The LDA consists in assuming that a local neutron Fermi momentum, $\hbar k_f(\mathbf{x})$, can be defined as a function of the neutron number density, $n(\mathbf{x})$, at that point. The (bound) protons, instead, decouple from the problem, only guaranteeing the existence of the neutron-rich nucleus. In order to achieve hydrostatic equilibrium of the neutrons, however, the total

Table 1
Physical parameters of the five zones of interest as calculated in Ref. [6]. The average baryon densities, ρ_B, are given in g/cm^3, the densities of the free neutron gas, n_G, in fm^{-3}, the radii of the WS-cells, $R_{\rm WS}$, those of the nuclei, R_N, and their diffusivities, a, in fm. The total number of neutrons in each cell, and the number of protons and neutrons bound in nuclei are indicated by N, Z and $N_{\rm bound}$, respectively. The number of unbound neutrons, renormalized to a cubic cell of side $L_{\rm WS} = 2R_{\rm WS}$, is indicated by $N'_{\rm free}$

Zone	1	2	3	4	5
ρ_B	1.5×10^{12}	9.6×10^{12}	3.4×10^{13}	7.8×10^{13}	1.3×10^{14}
n_G	4.8×10^{-4}	4.7×10^{-3}	1.8×10^{-2}	4.4×10^{-2}	7.4×10^{-2}
$R_{\rm WS}$	44.0	35.5	27.0	19.4	13.77
R_N	6.0	6.7	7.3	6.7	5.2
a	0.77	0.83	0.94	1.12	1.25
N	280	1050	1750	1460	950
Z	40	50	50	40	32
$N_{\rm bound}$	110	110	110	70	40
$N'_{\rm free}$	324	1795	3132	2654	1738

chemical potential μ of the system must be constant, independent of position. At $T = 0$, the chemical potential coincides with the Fermi energy; this zero-temperature case is a good approximation for the inner crust of a neutron star, due to the fact that the typical crust temperatures ($T \sim 0.01$ MeV) are much lower than the typical critical temperatures of pairing ($T_c \sim 0.5$ MeV). The Fermi energy of the neutrons in a WS-cell is given by the sum of local terms, $\mu_i(\mathbf{x})$, that are associated to the Fermi internal energy (i.e., calculated in the free Fermi gas model), to the nuclear energy coming from the central nucleus (and which accounts for the bound neutrons), to the kinetic energy arising from the vorticose superfluid motion and to the condensation energy due to the pairing of the superfluid neutrons. We remind that the last two terms are zero in the case of a normal phase. These local chemical potentials can be obtained from the corresponding energy densities in the standard way, that is $\mu_i(\mathbf{x}) = (\delta\varepsilon_i(\mathbf{x}))/(\delta n(\mathbf{x}))$. Note that the energy densities, $\varepsilon_i(\mathbf{x})$, depend on position through their dependence on the neutron number density. As for the (constant) gravitational term $\mu_{\rm grav} \sim -10^2$ MeV, due to core of the star and which guarantees that the system of neutrons is altogether bound, it is included as a shift in the Fermi energy μ which therefore results positive.

As already mentioned, in the LDA framework all quantities depend on position via the neutron local Fermi momentum $\hbar k_f(\mathbf{x})$, which is related to the number density of neutrons $n(\mathbf{x})$ by the usual expressions $3\pi^2 n(\mathbf{x}) = k_f(\mathbf{x})^3$. The four local chemical potentials are given below together with the corresponding energy density expressions. The Fermi internal terms are

$$\varepsilon_{\rm fer}(\mathbf{x}) = \frac{3}{5}\frac{\hbar^2 k_f^2(\mathbf{x})}{2m_n} n(\mathbf{x}), \qquad \mu_{\rm fer}(\mathbf{x}) = \frac{\hbar^2 k_f^2(\mathbf{x})}{2m_n}, \tag{1}$$

where m_n is the neutron mass. The nuclear terms due to a Woods–Saxon potential of depth U_0, radius R_N and diffusivity a are

$$\varepsilon_{\rm nuc}(\mathbf{x}) = \frac{-U_0}{1 + e^{\frac{r-R_N}{a}}} n(\mathbf{x}), \qquad \mu_{\rm nuc}(\mathbf{x}) = \frac{-U_0}{1 + e^{\frac{r-R_N}{a}}}, \tag{2}$$

where r is the distance from the center of the nucleus. The kinetic terms due to the irrotational motion around the vortex axis are

$$\varepsilon_{\rm kin}(\mathbf{x}) = \frac{\hbar^2}{8m_n R^2} n(\mathbf{x}), \qquad \mu_{\rm kin}(\mathbf{x}) = \frac{\hbar^2}{8m_n R^2}, \tag{3}$$

where R is the distance from the vortex axis. Finally, the pairing condensation terms are

$$\begin{aligned} \varepsilon_{\rm con}(\mathbf{x}) &= -\frac{3}{8}\frac{\Delta^2(\mathbf{x}) n(\mathbf{x})}{\mu_{\rm fer}(\mathbf{x})}, \\ \mu_{\rm con}(\mathbf{x}) &= -\frac{\Delta^2(\mathbf{x})}{8\mu_{\rm fer}(\mathbf{x})}\left[1 + 6\frac{n(\mathbf{x})}{\Delta(\mathbf{x})}\frac{\delta\Delta(\mathbf{x})}{\delta n(\mathbf{x})}\right], \end{aligned} \tag{4}$$

where the second term in the condensational chemical potential comes from the density dependence of the pairing gap, that is $\Delta(\mathbf{x}) = \Delta[n(\mathbf{x})]$.

The calculation requires choosing the neutron gap, that is the neutron pairing interaction. On the one hand, calculations of the energy gap based on realistic microscopic nucleon–nucleon interactions (e.g., Paris and Argonne interactions) have been performed, which have the problem of not considering the induced interaction produced by the surrounding medium of nucleons. On the other hand, effective potentials (e.g., Gogny and Skyrme interactions) have also been used, but these have been developed for ordinary finite nuclei and it is not clear how they work for bulk neutron-rich matter. The values of the gaps with effective interactions are generally larger than those with realistic potentials. Since the nature of the pairing interaction is not the issue we want to address in this paper, in what follows we will use the neutron pairing gaps obtained from Argonne's potential and Gogny's effective interaction as benchmarks.

For any *given* value of μ, one can determine the neutron density $n(\mathbf{x})$ for the normal and superfluid phases as a function of position in the cell using the Thomas–Fermi ansatz that the Fermi energy is independent on position. In particular, the density of the normal phase, $n_n(\mathbf{x})$, is obtained from the constraint

$$\mu = \mu_{\rm fer}(\mathbf{x}) + \mu_{\rm nuc}(\mathbf{x}), \tag{5}$$

while the density of the superfluid phase, $n_s(\mathbf{x})$, is derived from

$$\mu = \mu_{\rm fer}(\mathbf{x}) + \mu_{\rm nuc}(\mathbf{x}) + \mu_{\rm kin}(\mathbf{x}) + \mu_{\rm con}(\mathbf{x}). \tag{6}$$

From the calculated values of the neutron density, the total energy of the WS-cell can then be obtained for either phase by integration over the volume of the cell of the respective total energy densities, that is

$$\varepsilon_{{\rm tot},n}(\mathbf{x}) = \varepsilon_{\rm fer}(\mathbf{x}) + \varepsilon_{\rm nuc}(\mathbf{x}) \tag{7}$$

for the normal phase and

$$\varepsilon_{{\rm tot},s}(\mathbf{x}) = \varepsilon_{\rm fer}(\mathbf{x}) + \varepsilon_{\rm nuc}(\mathbf{x}) + \varepsilon_{\rm kin}(\mathbf{x}) + \varepsilon_{\rm con}(\mathbf{x}) \tag{8}$$

for the superfluid one.

One can also calculate the normal and superfluid pressures, using the standard definition

$$P(\mathbf{x}) = n^2(\mathbf{x})\frac{\delta[\varepsilon_{\rm tot}(\mathbf{x})/n(\mathbf{x})]}{\delta n(\mathbf{x})}. \tag{9}$$

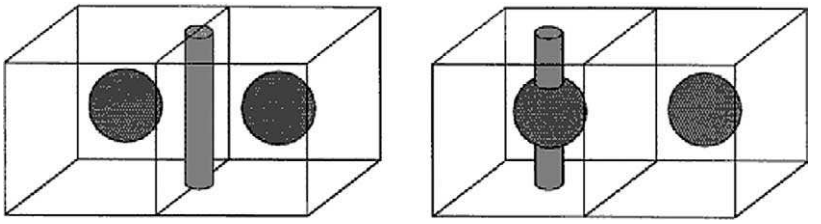

Fig. 1. The two vortex–nucleus configurations used in our calculation: interstitial pinning (IP, left) and nuclear pinning (NP, right). The cubes indicate the WS-cells, the spheres represent the nuclei in the middle of the cell and the cylinders picture the position of the vortex core.

The pressure in the normal phase is then equal to

$$P_n(\mathbf{x}) = \frac{2}{5}\frac{\hbar^2 k_{f,n}^2(\mathbf{x})}{2m_n} n_n(\mathbf{x}) = \frac{2}{5}\mu_{\mathrm{fer},n}(\mathbf{x}) n_n(\mathbf{x}), \tag{10}$$

while that in the superfluid phase is given by

$$P_s(\mathbf{x}) = \left[\frac{2}{5}\mu_{\mathrm{fer},s}(\mathbf{x}) + \frac{1}{4}\frac{\Delta^2(\mathbf{x})}{\mu_{\mathrm{fer},s}(\mathbf{x})} - \frac{3}{4}\frac{\Delta(\mathbf{x}) n_s(\mathbf{x})}{\mu_{\mathrm{fer},s}(\mathbf{x})}\frac{\delta\Delta(\mathbf{x})}{\delta n(\mathbf{x})}\right] n_s(\mathbf{x}). \tag{11}$$

We can now describe the vortex–nucleus configurations in our model. We start by considering two cubic WS-cells, over which we will integrate the energies, and we put them adjacent along a direction labeled as the x-axis. The vortex axis is aligned along the z direction. At the center of each cell we have a nucleus and in the leftmost one we put the origin of our Cartesian system of reference, so that the other nucleus lies on the x-axis. The nuclear pinning (NP) configuration has the vortex passing through the nucleus at the origin. The interstitial pinning (IP) configuration has the vortex equidistant between the two nuclei (see Fig. 1).

So far, when discussing the neutrons in the WS-cell we have implicitly assumed that they were all either in the normal phase (and thus without any vortex) or in the superfluid phase (with one vortex-line singularity in the NP or IP configuration). However, the usual hybrid state used in all previous calculations of pinning is also possible in the Thomas–Fermi approach, namely the neutrons in the cell can be superfluid everywhere except in the so-called vortex core, an axially symmetric region around the vortex axis where they are normal. In order to fulfill the condition of hydrostatic equilibrium of the model, the pressure of the normal phase must be equal to that of the superfluid one all along the boundary of the vortex core. The thermodynamical equilibrium is already guaranteed by taking the same μ for both phases.

More precisely, in the present semi-classical picture there are only two possible structures for a vortex which are consistent with mechanical equilibrium. The 'mixed' phase, in which an axially symmetric surface coaxial with the vortex, $S_M(z)$, is determined by the condition $P_s(\mathbf{x}) = P_n(\mathbf{x})$; in this phase matter is normal inside $S_M(z)$ and superfluid outside (normal core). The 'pure' phase, in which matter is always superfluid, but with its density going smoothly to zero along some other axially symmetric surface coaxial with the vortex, $S_P(z)$, determined by the condition $n_s(\mathbf{x}) = 0$; in this phase there are no neutrons inside $S_P(z)$ (empty core). We point out that the surfaces $S_M(z)$ and $S_P(z)$ unambiguously

describe the vortex cores in the two phases; the radii of their circular transverse sections depend on the z coordinate in the case of the NP configuration, where the nucleus breaks the symmetry along the vortex axis; conversely, $S_M(z)$ and $S_P(z)$ are basically cylinders in the IP configuration. We also observe that, in the case of the 'mixed' phase, while the neutron pressure is continuous along the surface $S_M(z)$, the neutron density and total energy density both present a discontinuity along it.

The thermodynamically stable phase actually chosen by the system will be the one with minimum total energy. This follows from the standard minimization condition for the Helmholtz free energy $F = E - TS$ (we are considering a system with fixed temperature, $T = 0$, and fixed volume, $V = 2L_{\mathrm{WS}}^3 = 16R_{\mathrm{WS}}^3$) and from the fact that $F = E$ at zero temperature.

3. Calculations and results

In this section we will show the results that are obtained when the model described above is applied to the five zones of the inner crust (see Table 1).

We first have to find, for each zone, the value of the constant Fermi energy μ which is needed to calculate the neutron density $n(\mathbf{x})$. Since, according to the Feynman–Onsager relation [2], the mean spacing between vortex lines is orders of magnitude larger than R_{WS} for even the fastest pulsars, we can take the vortices as isolated. Moreover, the $1/R^2$ behavior of the kinetic term guarantees that the effect of the vortex becomes negligible as one moves away from the vortex axis. Indeed, we find that the ratio $\mu_{\mathrm{kin}}(\mathbf{x})/\mu$ between the kinetic contribution and the Fermi energy is already as small as 10^{-3} at $R = R_{\mathrm{WS}}$, so that in practice the kinetic term can be neglected outside the WS-cell containing the vortex. Therefore, the vortex is actually surrounded by regular (without vortex) superfluid cells, which determine the constant value of μ. In other words, the surrounding cells act as a particle bath, which exchange neutrons with the vortex region in such a way as to maintain μ fixed. We therefore take a single superfluid cubic cell without vortex as the system from which to calculate μ.

The Fermi energy μ as well as the potential depth U_0 have then been obtained for each zone by an iterative procedure which integrates over a single vortex-free superfluid cell the density $n_0(\mathbf{x})$, calculated from Eq. (6) but *without* the kinetic term, in such a way as to get the required numbers of neutrons N_{bound} and N'_{free} that are, respectively, bound in or free from the nuclear potential. We notice that in the LDA the (effective) potential depth U_0 of the nuclear potential is calculated for each zone and it is determined by N_{bound} alone, once the nuclear radius and diffusivity are given. Using these values of μ, U_0 and the final neutron density $n_0(\mathbf{x})$, the total energy of a vortex-free cell, $E_{0,\mathrm{tot}}$, is obtained by integrating over the cell volume the total energy density of Eq. (8) (without the kinetic term). The results of this calculations are shown in Tables 2 and 3 for the Argonne and Gogny pairing gap, respectively.

Having determined the important physical parameters needed in our model, we can now proceed to analyze the nuclear and interstitial pinning configurations for each of the five zones of interest, and this for both Argonne and Gogny pairing gaps. This means that, as described above, we must calculate for each configuration the neutron density correspond-

Table 2
Physical parameters of the five zones in the inner crust calculated with Argonne pairing gap. The depth of the nuclear potential, U_0, and the Fermi energy, μ, are given in MeV. The energy terms for one cubic WS-cell without vortex are also reported in MeV and $E_{0,\mathrm{tot}} = E_{0,\mathrm{fer}} + E_{0,\mathrm{nuc}} + E_{0,\mathrm{con}}$

Zone	1	2	3	4	5
U_0	52.23	41.51	35.05	30.36	33.76
μ	1.02	5.45	14.32	24.82	36.79
$E_{0,\mathrm{fer}}$	2957.38	9166.78	31260.69	43369.09	41707.09
$E_{0,\mathrm{nuc}}$	−4430.99	−4371.73	−5606.30	−4907.10	−4159.78
$E_{0,\mathrm{con}}$	−40.20	−493.04	−568.60	−97.65	−2.84
$E_{0,\mathrm{tot}}$	−1513.82	4302.01	25085.79	38364.34	37544.46

Table 3
Physical parameters of the five zones in the inner crust calculated with Gogny pairing gap. See Table 2 for an explanation of the entries

Zone	1	2	3	4	5
U_0	52.21	41.47	34.97	30.19	33.40
μ	1.03	5.34	14.13	24.79	36.89
$E_{0,\mathrm{fer}}$	2952.55	9137.87	31202.18	43336.30	41694.28
$E_{0,\mathrm{nuc}}$	−4423.83	−4338.83	−5536.42	−4847.20	−4101.89
$E_{0,\mathrm{con}}$	−39.51	−578.50	−1014.51	−452.17	−87.40
$E_{0,\mathrm{tot}}$	−1510.79	4220.53	24651.25	38036.93	37504.98

ing to either the ‘pure’ phase (all superfluid neutrons) or the ‘mixed’ phase (superfluid and normal neutrons matched by the pressure condition). Of the two possibilities corresponding to a given configuration, the system will choose the one with minimum total energy, which we must determine case by case.

When comparing energies, however, one must remember that different configurations can have different number of particles in the fixed volume over which the energies are integrated (from now on, the two adjacent cubic WS-cells); this is a consequence of fixing the value for the chemical potential. Although the fractional changes in total particle number ($\Delta N/N$) are quite small, the effect on the total energy cannot be neglected when studying the vortex–nucleus interaction. This is the point we have overlooked in Ref. [8], and which led to incorrect conclusions about the pinning. Now, if the number of particles N in a fixed volume changes by ΔN, one must account for their additional energy in order to compare systems with equal particle number. Since these ΔN particles are exchanged with the particle bath, one must add to the total energy of the volume a term $\Delta E_\mu = -\mu \Delta N$. Of course, this is equivalent to the standard formal procedure of minimizing the expectation value of the operator $\hat{H}' = \hat{H} - \mu \hat{N}$, instead of that of the Hamiltonian $\hat{H}$ alone, when the particle number is not fixed.

The results are summarized in six tables. In Tables 4 to 7 the energies for the vortex–nucleus configurations are given relative to the values corresponding to a system of *two* vortex-free cells. Therefore, we actually list the differences δE between the energy of two cells with and without vortex. In the last line we indicate the phase with minimum total energy. In Tables 8 and 9 we give the calculated radii of the vortex core at its center (in the

Table 4
Results for the 'pure' (P) and 'mixed' (M) phases, calculated with Argonne pairing gap in the NP configuration. The energies are reported as differences δE between the energy of two cells with and without vortex, they are given in MeV and $\delta E_{\rm tot} = \delta E_{\rm fer} + \delta E_{\rm nuc} + \delta E_{\mu} + \delta E_{\rm kin} + \delta E_{\rm con}$. The last line indicates the phase with minimum total energy

	Nuclear pinning (Argonne)				
Zone	1	2	3	4	5
$\delta E_{\rm fer}$ (M)	−4.66	−35.38	−54.84	76.34	6.18
$\delta E_{\rm fer}$ (P)	−187.44	−228.52	−365.09	−449.50	−497.22
$\delta E_{\rm nuc}$ (M)	−0.55	−1.47	−2.46	−2.38	−0.18
$\delta E_{\rm nuc}$ (P)	201.55	175.48	175.38	147.58	135.16
δE_{μ} (M)	4.56	35.25	57.55	−74.10	−6.03
δE_{μ} (P)	10.50	78.70	230.12	351.99	419.26
$\delta E_{\rm kin}$ (M)	3.29	21.83	42.13	5.52	0.00
$\delta E_{\rm kin}$ (P)	98.96	124.50	205.50	249.53	273.99
$\delta E_{\rm con}$ (M)	2.83	8.25	14.69	22.76	0.62
$\delta E_{\rm con}$ (P)	0.95	2.72	0.42	−0.65	−0.10
$\delta E_{\rm tot}$ (M)	5.46	28.49	57.08	28.14	0.59
$\delta E_{\rm tot}$ (P)	124.52	152.88	246.34	298.96	331.09
Phase	M	M	M	M	M

Table 5
Results for the 'pure' (P) and 'mixed' (M) phases, calculated with Argonne pairing gap in the IP configuration. See Table 4 for an explanation of the entries

	Interstitial pinning (Argonne)				
Zone	1	2	3	4	5
$\delta E_{\rm fer}$ (M)	−5.27	−40.49	−69.05	91.45	8.87
$\delta E_{\rm fer}$ (P)	−6.14	−55.22	−166.39	−267.03	−324.60
$\delta E_{\rm nuc}$ (M)	0.01	0.04	0.12	−0.60	−0.04
$\delta E_{\rm nuc}$ (P)	0.01	0.04	−0.12	0.38	1.31
δE_{μ} (M)	4.63	38.75	69.00	−91.15	−8.81
δE_{μ} (P)	5.87	57.69	182.53	295.37	359.27
$\delta E_{\rm kin}$ (M)	2.16	21.23	45.16	5.22	0.00
$\delta E_{\rm kin}$ (P)	2.96	31.67	98.05	149.67	179.92
$\delta E_{\rm con}$ (M)	1.30	7.41	17.06	28.28	0.93
$\delta E_{\rm con}$ (P)	0.93	3.20	0.85	−0.89	−0.18
$\delta E_{\rm tot}$ (M)	2.83	26.94	62.29	33.20	0.94
$\delta E_{\rm tot}$ (P)	3.62	37.37	114.92	177.50	215.71
Phase	M	M	M	M	M

two configurations and for both phases), that is of the normal circular sections of $S_M(z)$ and $S_P(z)$ at $z = 0$. We also report the associated coherence lengths $\xi(z)$ (for both configurations and again at $z = 0$), defined as the radii of the surface where $\varepsilon_{\rm kin}(\mathbf{x}) = |\varepsilon_{\rm con}(\mathbf{x})|$, a natural extension of the standard constant-density definition. In this respect, we point out that from Eqs. (1)–(11) and after some algebra one obtains $\Delta P = -\Delta\varepsilon_{\rm tot} + \mu\Delta n$, where $\Delta P = P_s(\mathbf{x}) - P_n(\mathbf{x})$, $\Delta\varepsilon_{\rm tot} = \varepsilon_{{\rm tot},s}(\mathbf{x}) - \varepsilon_{{\rm tot},n}(\mathbf{x})$ and $\Delta n = n_s(\mathbf{x}) - n_n(\mathbf{x})$ (this also follows directly from the definition at $T = 0$ of the thermodynamical potential per

Table 6
Results for the 'pure' (P) and 'mixed' (M) phases, calculated with Gogny pairing gap in the NP configuration. See Table 4 for an explanation of the entries

	Nuclear pinning (Gogny)				
Zone	1	2	3	4	5
$\delta E_{\rm fer}$ (M)	−1.09	−33.19	−69.45	−31.34	71.26
$\delta E_{\rm fer}$ (P)	−187.62	−228.60	−362.92	−444.77	−497.02
$\delta E_{\rm nuc}$ (M)	−4.34	−6.83	−8.74	−7.55	−4.01
$\delta E_{\rm nuc}$ (P)	201.61	174.86	174.38	146.60	134.27
δE_{μ} (M)	4.76	37.62	77.27	39.10	−67.22
δE_{μ} (P)	10.70	78.35	227.01	347.83	420.37
$\delta E_{\rm kin}$ (M)	4.52	24.52	53.25	43.11	0.00
$\delta E_{\rm kin}$ (P)	98.87	123.76	204.11	248.76	273.73
$\delta E_{\rm con}$ (M)	5.62	13.45	20.90	25.18	22.26
$\delta E_{\rm con}$ (P)	0.86	3.63	2.09	−0.42	−0.60
$\delta E_{\rm tot}$ (M)	9.46	35.57	73.24	68.50	22.29
$\delta E_{\rm tot}$ (P)	124.41	152.00	244.66	298.00	330.75
Phase	M	M	M	M	M

Table 7
Results for the 'pure' (P) and 'mixed' (M) phases, calculated with Gogny pairing gap in the IP configuration. See Table 4 for an explanation of the entries

	Interstitial pinning (Gogny)				
Zone	1	2	3	4	5
$\delta E_{\rm fer}$ (M)	−5.36	−44.21	−95.94	−59.90	79.65
$\delta E_{\rm fer}$ (P)	−6.22	−56.63	−167.11	−262.35	−324.15
$\delta E_{\rm nuc}$ (M)	0.01	0.12	−0.11	0.27	−0.86
$\delta E_{\rm nuc}$ (P)	0.01	0.05	−0.04	0.29	1.31
δE_{μ} (M)	4.75	41.58	94.78	59.86	−78.89
δE_{μ} (P)	6.02	58.01	180.88	289.81	359.41
$\delta E_{\rm kin}$ (M)	2.04	21.87	54.62	48.19	0.00
$\delta E_{\rm kin}$ (P)	2.93	31.50	98.04	150.21	180.27
$\delta E_{\rm con}$ (M)	1.26	8.27	18.16	27.53	28.25
$\delta E_{\rm con}$ (P)	0.86	4.29	3.23	0.02	−0.77
$\delta E_{\rm tot}$ (M)	2.70	27.63	71.51	75.96	28.16
$\delta E_{\rm tot}$ (P)	3.61	37.22	115.00	177.98	216.08
Phase	M	M	M	M	M

unit volume $\omega = \varepsilon_{\rm tot} - \mu n = -P$). In the simple constant-density models one has $\Delta n = 0$ everywhere so that the condition $\Delta P = 0$, which defines the vortex core in the 'mixed' phase (i.e., the surface where the two phases are in thermodynamical and mechanical equilibrium), is equivalent to $\Delta\varepsilon_{\rm tot} = 0$, namely that the total energy density is continuous at the phase interface. In turn, this implies $\varepsilon_{\rm kin}(\mathbf{x}) = |\varepsilon_{\rm con}(\mathbf{x})|$ since $n_s = n_n$; therefore, if the density variations are neglected, our definition of the vortex core is equivalent to the standard definition of the coherence length. In the general case with varying density, instead, the condition $\Delta P = 0$ implies that $\Delta\varepsilon_{\rm tot} - \mu\Delta n = \Delta\omega = 0$, which is the correct quantity to be continuous at the phase interface for a system with fixed volume and variable particle

Table 8
Radii of the vortex core and coherence lengths calculated at $z = 0$ with Argonne pairing gap. The central radii $r_c(P)$ and $r_c(M)$ of the 'pure' and 'mixed' phases and the central coherence length $\xi(0)$ are evaluated for the NP and IP configurations, and are given in fm

	r_c (P)		r_c (M)		$\xi(0)$	
Zone	NP	IP	NP	IP	NP	IP
1	0.32	2.30	6.54	7.10	6.54	7.02
2	0.34	0.98	7.26	4.34	7.25	4.34
3	0.33	0.61	8.55	5.22	8.54	5.20
4	0.31	0.46	11.77	11.38	11.71	11.30
5	0.28	0.38	8.62	8.62	8.62	8.62

Table 9
Radii of the vortex core and coherence lengths calculated at $z = 0$ with Gogny pairing gap. See Table 8 for an explanation of the entries

	r_c (P)		r_c (M)		$\xi(0)$	
Zone	NP	IP	NP	IP	NP	IP
1	0.32	2.25	5.98	7.91	5.97	7.76
2	0.34	0.99	6.47	4.08	6.46	4.07
3	0.33	0.61	7.30	3.94	7.29	3.93
4	0.31	0.46	7.79	5.35	7.78	5.33
5	0.28	0.38	8.62	8.62	8.62	8.62

number (the potential $\omega = \varepsilon_{\text{tot}} - \mu n$ is the energy density associated to the Hamiltonian $\hat{H}' = \hat{H} - \mu\hat{N}$).

We now make a few observations about these intermediate results:

(i) The 'mixed' phase is always favored in the LDA. Such a vortex structure, that was assumed without explanation in all previous calculations of pinning, is thus justified in the LDA by energy considerations. We point out that this result follows from the inclusion of all energy terms, none of them being negligible in magnitude as compared to the others.

(ii) The fact that in several cases $\delta E_{\text{tot}} > 0$ (i.e., the system of two WS-cells has a lower energy when no vortex is present) should not surprise, because the existence of vortices follows from global *macroscopic* energy arguments, not on the local energy balance of two cells.

(iii) The vortex cores are about one order of magnitude larger in the 'mixed' phase than in the 'pure' one. Since the LDA is known to describe poorly the low-density tail of a system, it is satisfying that in the subsequent calculations we have to use always the 'mixed' phase, whose density never goes to zero. When compared to the corresponding coherence lengths, instead, the radii of the normal cores differ by less than one percent. Therefore, the simple assumption of a core radius equal to ξ is actually a good approximation. We expect that, in a complete quantum calculation, this will translate into an order parameter (e.g., the gap) going to zero over a length scale of order ξ.

Table 10
Difference in total number of neutrons $\Delta N = N^{(\mathrm{NP})} - N^{(\mathrm{IP})}$ and energy differences $\Delta E = E^{(\mathrm{NP})} - E^{(\mathrm{IP})}$ between the configuration with nuclear pinning and that with interstitial pinning, calculated with Argonne pairing gap. The energies are given in MeV and $\Delta E_{\mathrm{tot}} = \Delta E_{\mathrm{int}} + \Delta E_{\mathrm{kin}} + \Delta E_{\mathrm{con}}$, where the internal contribution is defined as $\Delta E_{\mathrm{int}} = \Delta E_{\mathrm{fer}} + \Delta E_{\mathrm{nuc}} + \Delta E_{\mu}$

	Argonne				
Zone	1	2	3	4	5
ΔN	0.06	0.64	0.80	−0.69	−0.08
ΔE_{fer}	0.61	5.11	14.22	−15.10	−2.68
ΔE_{nuc}	−0.56	−1.51	−2.58	−1.79	−0.14
ΔE_{μ}	−0.07	−3.50	−11.45	17.05	2.78
ΔE_{int}	−0.02	0.10	0.19	0.16	−0.04
ΔE_{kin}	1.12	0.61	−3.03	0.30	0
ΔE_{con}	1.53	0.84	−2.37	−5.52	−0.31
ΔE_{tot}	2.6	1.6	−5.2	−5.1	−0.4

Table 11
Difference in total number of neutrons $\Delta N = N^{(\mathrm{NP})} - N^{(\mathrm{IP})}$ and energy differences $\Delta E = E^{(\mathrm{NP})} - E^{(\mathrm{IP})}$ between the configuration with nuclear pinning and that with interstitial pinning, calculated with Gogny pairing gap. See Table 10 for an explanation of the entries

	Gogny				
Zone	1	2	3	4	5
ΔN	−0.01	0.74	1.24	0.84	−0.32
ΔE_{fer}	4.27	11.02	26.49	28.56	−8.40
ΔE_{nuc}	−4.35	−6.94	−8.63	−7.82	−3.15
ΔE_{μ}	0.01	−3.97	−17.51	−20.75	11.66
ΔE_{int}	−0.07	0.11	0.35	−0.01	0.11
ΔE_{kin}	2.48	2.65	−1.36	−5.09	0
ΔE_{con}	4.36	5.17	2.74	−2.35	−5.99
ΔE_{tot}	6.8	7.9	1.7	−7.5	−5.9

We are finally able to evaluate the difference in energy between the nuclear pinning and the interstitial pinning configurations for each zone in the case of Argonne and Gogny pairing gap, taking always the 'mixed' structure for the vortex. The results are reported in three tables. In Tables 10 and 11 we list the differences $\Delta E = E^{(\mathrm{NP})} - E^{(\mathrm{IP})}$ between the NP and the IP configurations for both pairing interactions. For sake of comparison with previous calculations, we define the difference in internal contribution as $\Delta E_{\mathrm{int}} = \Delta E_{\mathrm{fer}} + \Delta E_{\mathrm{nuc}} + \Delta E_{\mu}$, namely all terms other than kinetic and condensational, so that $\Delta E_{\mathrm{tot}} = \Delta E_{\mathrm{int}} + \Delta E_{\mathrm{kin}} + \Delta E_{\mathrm{con}}$. Obviously, ΔE_{tot} represent the quantity of interest to us, namely the pinning energy. When $\Delta E_{\mathrm{tot}} < 0$ the vortex pins to the nucleus, that is nuclear pinning is favored energetically.

In Table 12 we compare the (nuclear) pinning energies, E_{NP}, and the average (nuclear) pinning forces, F_{NP}, obtained from our calculation to previous results found in the literature, in particular those coming from the Landau–Ginzburg approximation [4]. The pinning force is actually the physical quantity that appears in model calculations trying to explain pulsar glitches by vortex unpinning. Since ΔE_{tot} represents the difference in energy be-

Table 12
Comparison of the (nuclear) pinning energies, $E_{\rm NP}$, and of the average (nuclear) pinning forces, $F_{\rm NP}$, calculated in this work for the Argonne and Gogny pairing interaction and those obtained in Ref. [9] from the data of Ref. [4]. The energies are given in MeV, the forces in MeV/fm, while '–' indicates interstitial pinning

	$E_{\rm NP}$			$F_{\rm NP}$		
Zone	Argonne	Gogny	Ref. [9]	Argonne	Gogny	Ref. [9]
1	–	–	–	–	–	–
2	–	–	0.4	–	–	0.11
3	5.2	–	15	0.19	–	3.6
4	5.1	7.5	9	0.26	0.38	1.9
5	0.4	5.9	5.4	0.03	0.43	1.7

tween two configurations where the vortex has been moved by a distance $R_{\rm WS}$, the average (nuclear) pinning force per (nuclear) pinning site is naturally defined as

$$F_{\rm NP} = \frac{E_{\rm NP}}{R_{\rm WS}}, \qquad E_{\rm NP} = |\Delta E_{\rm tot}|. \tag{12}$$

This definition holds only for the case of nuclear pinning, that is when $\Delta E_{\rm tot} < 0$. Indeed, when interstitial pinning occurs the pinning force is orders of magnitude smaller than what one would obtain from Eq. (12), as discussed in Ref. [9] where it was found that $F_{\rm IP} \sim 10^{-5}$–10^{-3} MeV/fm depending on the density. Consequently we have reported the pinning forces only for the case of pinning on nuclei.

The results presented in the last tables deserve some comments:

(i) As before, none of the energy terms is negligible in magnitude as compared to the others. In particular, although the change in total number of neutrons is very small, the associated change in energy ΔE_μ can be quite large.
(ii) When the terms $\Delta E_{\rm fer}$, $\Delta E_{\rm nuc}$ and ΔE_μ are summed up in $\Delta E_{\rm int}$, this internal contribution is small in magnitude as compared to the remaining kinetic and condensational terms, $\Delta E_{\rm kin}$ and $\Delta E_{\rm con}$. Therefore, as a first rough approximation one could neglect the internal contribution.
(iii) Nuclear pinning occurs only in zones 3 to 5 ($\rho > 3.4 \times 10^{13}$ g/cm^3) with the Argonne gap and in zones 4 and 5 ($\rho > 7.8 \times 10^{13}$ g/cm^3) with the Gogny gap. When compared to the results of Ref. [4], who found pinning on nuclei in zones 2 to 5 ($\rho > 9.6 \times 10^{12}$ g/cm^3), we see that the LDA predicts nuclear pinning only in a limited density range.
(iv) The average (nuclear) pinning forces are small and altogether quite independent in magnitude from the pairing interaction used. Comparing $E_{\rm NP}$ and $F_{\rm NP}$ to the results of the Landau–Ginzburg approximation [4] (where an interaction very similar to Argonne was used), we see that the LDA predicts quite weak nuclear pinning.
(v) The results listed for the average forces represent a lower bound for the real (nuclear) pinning forces as a function of distance from the nucleus. To calculate the latter, however, one would have to deal with a less symmetric and thus more complicated problem.
(vi) When computing the kinetic energy contribution due to vorticose motion, we introduce a cut-off for hydrodynamical consistency. Namely, we assume a $1/R$ velocity

profile only for $R < R_{\rm WS} - R_N$ (and zero outside) in order not to violate the continuity equation at the nucleus in the IP configuration. This means that the results for $\Delta E_{\rm kin}$ (and thence for $\Delta E_{\rm tot}$) should be corrected, to account for the effect of the nucleus on the neutron flow in the IP configuration. An analytical calculation was performed in Ref. [4] for a constant-density nucleus far away from the vortex line, and it can be used to evaluate the order of magnitude of such a correction. We found that one should subtract from $\Delta E_{\rm tot}$ a small correction ($\leqslant 0.1$ MeV). To point out this known uncertainty, in the last line of Tables 10 and 11 we reported the energies rounding them off to one decimal figure.

4. Conclusions

We have presented in full detail the first fully consistent and realistic treatment of vortex–nucleus interaction in the inner crust of neutron stars. Within the framework of the local density approximation, the model determines the configurations with lowest energy, while ensuring thermodynamical and mechanical equilibrium. The main conclusions of the present work can be summarized as follows:

(i) The most stable structure for a vortex is that with a core made of normal matter, whose radius is very close to the local superfluid coherence length $\xi(z)$.
(ii) The nature of pinning (nuclear or interstitial) is determined mostly by the kinetic and condensational contributions. The internal term gives only a small correction, negligible at a first rough approximation.
(iii) Pinning on nuclei appears only in a quite limited density range, when compared to previous studies.
(iv) The average (nuclear) pinning forces are quite small, when compared to previous studies.
(v) The nuclear pinning properties are not too sensitive to the pairing interaction used. Argonne gives nuclear pinning at somewhat lower densities, while Gogny gives slightly larger pinning forces.

Of course, these results also require some caveats. The main one is the semi-classical nature of the model which cannot describe the proximity effects due to the non-local nature of pairing. In that respect, a complete quantum calculation is needed. The work of Ref. [10], based on the nuclear energy density functional approach, is a promising step in that direction. Another issue is the real nature of the pairing interaction in the exotic matter found in the inner crust of neutron stars, where neutron-rich heavy nuclei co-exist with unbound superfluid neutrons. Finally, we must remember that the pinning forces we obtained here are only average values, lower bounds to the maximum value of the distance-dependent force $F_{\rm NP}(s)$ (with s the distance between vortex and nucleus); this maximum value is what must be overcome by the Magnus force in order to actually unpin the vortex. We plan to address this issue within the framework of the LDA in a future paper.

The conclusions reached in the present paper are likely to be relevant for any explanation of pulsar glitches based on depinning of vortices from the nuclear lattice. Therefore, the

(nuclear) pinning energies obtained here should be introduced as an input in macroscopic models for vortex depinning. Whether this will improve the agreement between theory and observations, or rather make it impossible, is a fully open issue.

References

[1] P.W. Anderson, N. Itoh, Nature 256 (1975) 25.
[2] R.P. Feynman, Statistical Mechanics, Addison–Wesley, New York, 1972.
[3] M.A. Alpar, Astrophys. J. 213 (1977) 527.
[4] R. Epstein, G. Baym, Astrophys. J. 328 (1988) 680.
[5] P.M. Pizzochero, et al., Phys. Rev. Lett. 79 (1997) 3347.
[6] J.W. Negele, D. Vautherin, Nucl. Phys. A 207 (1973) 298.
[7] P.M. Pizzochero, et al., Astrophys. J. 569 (2002) 381.
[8] P. Donati, P.M. Pizzochero, Phys. Rev. Lett. 90 (2003) 211101.
[9] B. Link, R. Epstein, Astrophys. J. 373 (1991) 592.
[10] Y. Yu, A. Bulgac, Phys. Rev. Lett. 90 (2003) 161101.